miR-221 Is Required for Endothelial Tip Cell Behaviors during Vascular Development

Stefania Nicoli,[1,4] Carl-Philipp Knyphausen,[1,3] Lihua J. Zhu,[1,2] Abirami Lakshmanan,[1] and Nathan D. Lawson[1,*]

[1]Program in Gene Function and Expression
[2]Program in Bioinformatics and Integrative Biology
University of Massachusetts Medical School, Worcester, MA 01605, USA
[3]Westfälische Wilhelms-Universität Münster, Schlossplatz 2, D-48149 Münster, Germany
[4]Present address: Department of Medicine, Yale Cardiovascular Research Center, New Haven, CT 06511, USA
*Correspondence: nathan.lawson@umassmed.edu
DOI 10.1016/j.devcel.2012.01.008

SUMMARY

Angiogenesis requires coordination of distinct cell behaviors between tip and stalk cells. Although this process is governed by regulatory interactions between the vascular endothelial growth factor (Vegf) and Notch signaling pathways, little is known about the potential role of microRNAs. Through deep sequencing and functional screening in zebrafish, we find that *miR-221* is essential for angiogenesis. *miR-221* knockdown phenocopied defects associated with loss of the tip cell-expressed Flt4 receptor. Furthermore, *miR-221* was required for tip cell proliferation and migration, as well as tip cell potential in mosaic blood vessels. *miR-221* knockdown also prevented "hyper-angiogenesis" defects associated with Notch deficiency and *miR-221* expression was inhibited by Notch signaling. Finally, *miR-221* promoted tip cell behavior through repression of two targets: *cyclin dependent kinase inhibitor 1b* (*cdkn1b*) and *phosphoinositide-3-kinase regulatory subunit 1* (*pik3r1*). These results identify *miR-221* as an important regulatory node through which tip cell migration and proliferation are controlled during angiogenesis.

INTRODUCTION

During embryogenesis, vascular development proceeds through two distinct stages (Poole and Coffin, 1989). De novo formation of blood vessels, or vasculogenesis, begins with the emergence of angioblast progenitor cells from the lateral mesoderm and migration to target tissues where they coalesce, assemble into cords, and lumenize to form the major blood vessels. Subsequently, smaller caliber vessels sprout from pre-existing ones by angiogenesis (Poole and Coffin, 1989), which requires careful orchestration of distinct cell behaviors between adjacent endothelial cells (Gerhardt et al., 2003). Initial sprouting is driven by proangiogenic factors in the surrounding extracellular environment that induce selected cells to emerge from an established blood vessel. These leading tip cells exhibit extensive filopodia and pathfinding behavior, whereas trailing stalk cells do not (Gerhardt et al., 2003). In some vascular beds (e.g., mouse retinal

vasculature), the vascular plexus grows via proliferation of stalk cells as tip cells migrate, whereas in others (e.g., zebrafish segmental vessels) tip cells exhibit both migration and proliferation (Gerhardt et al., 2003; Siekmann and Lawson, 2007). Despite these differences, the distinction between tip and stalk cells is an essential conserved process that allows blood vessels to grow while maintaining their connection to the patent vascular system (Thurston et al., 2007).

The signals that coordinate tip and stalk cell behaviors have been the subject of intense investigation. Initial tip cell emergence is driven by Vascular endothelial growth factor A (Vegfa), which is acutely required for tip cell filopodia activity and migration (Gerhardt et al., 2003). Accordingly, tip cells express receptors for both Vegfa (Vegfr-2) and Vegfc (Vegfr-3/Flt4), the latter of which is highly dynamic and becomes restricted to the tip cell during sprouting (Covassin et al., 2006b; Gerhardt et al., 2003; Siekmann and Lawson, 2007; Tammela et al., 2008). Vegfa induces tip cell expression of the Notch ligand, *dll4*, and subsequent Notch activation in the stalk cell suppresses tip cell behaviors, in part, by repressing *flt4* expression (Hellström et al., 2007; Lobov et al., 2007; Siekmann and Lawson, 2007; Tammela et al., 2008). Consistent with this model, mouse or zebrafish embryos lacking *dll4* display excessive blood vessel branching and endothelial proliferation (Hellström et al., 2007; Leslie et al., 2007; Siekmann and Lawson, 2007; Suchting et al., 2007), which can be normalized by reducing Vegfr-3/flt4 signaling (Hogan et al., 2009; Siekmann and Lawson, 2007; Tammela et al., 2008). More recent observations have demonstrated competition between endothelial cells for the leading tip cell position during sprouting (Jakobsson et al., 2010). Endothelial cells with lower Vegfr-2 or increased Notch signaling are often excluded from the tip cell position (Jakobsson et al., 2010), consistent with similar results in mosaic zebrafish blood vessels (Siekmann and Lawson, 2007). Thus, tip and stalk cell behaviors are coordinated through negative interactions between the Vegf and Notch pathways. However, little is known about the possible role of posttranscriptional control of this dynamic process.

MicroRNAs are expressed as autonomous transcripts, or are found in introns where they are expressed within pre-mRNA (Ghildiyal and Zamore, 2009). Autonomous microRNA precursors are cleaved in the nucleus by Drosha (Lee et al., 2003), leaving short hairpin RNAs that are transported to the cytoplasm and cleaved by the ribonuclease Dicer (Bernstein et al., 2001; Hutvágner et al., 2001). The mature strand from the resulting double stranded ~22 nucleotide microRNA is subsequently
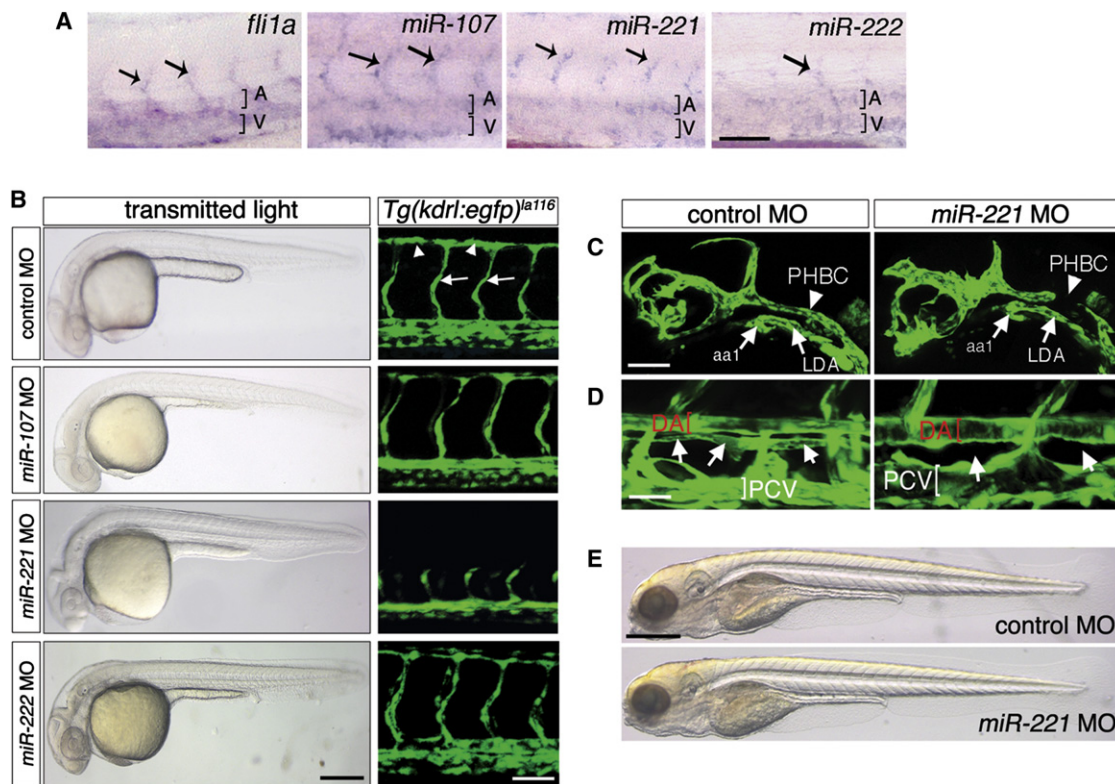
Figure 1. *miR-221* Is Required for Vascular Development

(A) Whole-mount in situ hybridization of embryos at 48 hr postfertilization (hpf). Dorsal aorta and posterior cardinal vein are indicated by a bracket and A or V, respectively. Arrows indicate intersegmental blood vessels (ISV). Scale bar = 50 μm.

(B) Left column, transmitted light images of embryos at 30 hpf injected with indicated MO. Scale bar = 250 μm. Right column, confocal micrographs of trunk vessels at 30 hpf in *Tg(kdrl:egfp)^la116* embryos injected with indicated MO. ISVs indicated by arrows and DLAV by arrowheads. Scale bar = 50 μm.

(C) *Tg(kdrl:egfp)^la116* embryos at 27 hpf injected with 10 ng control or *miR-221* MO. aa1, aortic arch 1; PHBC, primordial hindbrain channel; LDA, lateral dorsal aorta. Scale bar = 50 μm.

(D) *Tg(fli1a:egfp)^y1* embryos at 5 days postfertilization (dpf) injected as in (C). DA, dorsal aorta; PCV, posterior cardinal vein; position of thoracic duct is indicated by arrows. Scale bar = 25 μm.

(E) Transmitted light images of larvae at 5 dpf injected as in (C). Scale bar = 500 μm. All panels are lateral views, dorsal is up, anterior to the left.

incorporated into a ribonucleoprotein silencing complex (RISC; Czech and Hannon, 2011; Gregory et al., 2005) and used as a complementary guide sequence that binds to sites in the 3′ UTR of a target mRNA. Upon RISC binding, a target transcript is deadenylated leading to its degradation and translational repression (Giraldez et al., 2006; Guo et al., 2010; Wu et al., 2006). Thus, in most cases, microRNAs provide a mechanism for posttranscriptional repression of gene expression. Since microRNAs have been implicated in multiple aspects of vascular growth control (Suárez and Sessa, 2009), we reasoned that they might play a role to coordinate tip and stalk cell behaviors. By applying deep sequencing and functional screening of micro-RNAs in zebrafish embryos, we identified *mir-221* as an essential regulator of tip cell proliferation and migration.

RESULTS

miR-221 Is Expressed in Embryonic Endothelial Cells and Is Required for Angiogenesis

To identify candidate microRNAs required for angiogenesis, we sequenced small RNAs from zebrafish endothelial cells at 24 hr

postfertilization (hpf), at which time there is extensive vascular growth (Isogai et al., 2003; Siekmann and Lawson, 2007; Figure S1A available online). Approximately 20 microRNAs displayed 2-fold or greater enrichment in green fluorescent protein (GFP)+ cells isolated from *Tg(kdrl:egfp)^la116* embryos compared to GFP− cells and more than 50 were highly ex-pressed (>1,000 sequence tags) in GFP+ cells, many of which are also expressed in human endothelial cells (Table S1; Kueh-bacher et al., 2007). We also noted hematopoietic-expressed microRNAs (e.g., *miR-223*, *miR-451*) consistent with *kdrl:egfp* expression in hematopoietic cells (Bertrand et al., 2010).

We validated candidate microRNA expression by whole-mount in situ hybridization using locked nucleic acid (LNA) probes. Candidates were selected based on enrichment (e.g., *miR-20b*) or high expression (e.g., *miR-221*) in *kdrl:gfp*-positive cells. Several candidate microRNAs displayed expression similar to the endothelial-expressed transcription factor, *fli1a*, at 48 hpf including *miR-107*, *miR-20b*, *miR-221*, and *miR-222* (Figure 1A; Table S1; data not shown). To assess the function of these microRNAs, we injected Morpholinos (MOs) to block their maturation (Figure S1B and data not shown) and observed

vascular and overall morphology in *Tg(kdrl:egfp)^la116* embryos. In most cases, we noted normal development and intersegmental vessel (ISV) formation at 30 hpf, except for *miR-221* knockdown, which caused partial ISV formation (Figure 1B). We also observed distinct cardiovascular defects associated with loss of other microRNAs. For example, *miR-107*-deficient embryos displayed vascular stability defects (Figure S1C), whereas embryos lacking *miR-20b* exhibited an apparent block in erythroid differentiation (Figure S1D). Based on our interest in identifying microRNAs involved in angiogenesis, we investigated the function of *miR-221* in greater detail.

Consistent with our deep sequencing data, *miR-221* is detected at high levels in endothelial cells from *Tg(kdrl:egfp)^la116* embryos at 24 hpf (Figure S1E). Although a high proportion of *miR-221*-deficient embryos displayed partial ISV formation at 30 hpf (Figure 1B; Figure S1F), general embryonic development was not delayed and overall morphology appeared normal (Figure 1B). Loss of *miR-221* did not perturb development or differentiation of structures adjacent to ISVs, such as somites, neural tube, and notochord (Figure S1G). Closer inspection revealed defects in formation of the primordial hindbrain channel, a transient vein in the zebrafish hindbrain (Isogai et al., 2003), in embryos lacking *miR-221*, whereas the adjacent lateral dorsal aortae formed normally (Figure 1C). We also noted lack of the thoracic duct, a primary lymphatic vessel, at 5 days postfertilization, whereas overall morphology was normal at this stage (Figures 1D and 1E). A second MO targeting *miR-221* caused the same vascular defects (Figures S1H and S1I and data not shown). Although there is a high degree of homology between *miR-221* and *miR-222*, both MOs were specific for *miR-221* (Figure S1J) and simultaneous knockdown of *miR-221* and *miR-222* did not enhance or cause additional vascular defects (data not shown). We did not note any changes in expression of either *vegfa*, or its receptor *kdrl* (Figure S2A), which are essential for ISV sprouting, (Covassin et al., 2006b) in *miR-221*-deficient embryos. Likewise, ISV and vein-specific expression of *flt4* and artery-specific expression of its ligand *vegfc*, as well as *ephrinb2a, notch3,* and *dll4* were not affected by loss of *miR-221* (Figures S2A and S2B). Circulation and heart function were also normal in *miR-221*-deficient embryos (data not shown). Together, these results demonstrate that *miR-221* is highly expressed in endothelial cells and is required for angiogenesis.

miR-221 Is Required for Signaling through the Vegfc/Flt4 Pathway

In the zebrafish embryo, *kdrl* and *flt4* cooperate to drive ISV growth, whereas *flt4* alone is required for vein and lymphatic development and *kdrl* alone is required for artery differentiation and morphogenesis (Covassin et al., 2006b; Habeck et al., 2002; Hogan et al., 2009). Strikingly, the phenotypes associated with loss of *miR-221* were identical to those in embryos lacking *flt4* (Covassin et al., 2006b; Hogan et al., 2009). By contrast, *miR-221*-deficient embryos did not display hallmarks of Vegfa deficiency, such as arteriovenous circulatory shunts or loss of artery differentiation (data not shown; Figure S2A). These observations suggested that *miR-221* preferentially affects the Vegfc/Flt4 pathway. To determine if this was the case, we first assessed the genetic interaction between *miR-221* and *kdrl* or *flt4* by quantifying ISV length in embryos lacking combinations

of these genes. Embryos injected separately with either 1 ng of *flt4* or 5 ng of *miR-221* MO displayed ISVs of normal length at 30 hpf similar to embryos injected with control MO (Figures 2A–2C and 2G). However, coinjection of these subphenotypic MO doses resulted in significantly shorter ISVs (Figures 2D and 2G), similar to a more complete knockdown of either gene alone at higher doses (Figure 2G). Furthermore, we did not observe any enhancement of the ISV defect in embryos co-injected with these higher MO doses (Figure 2G), suggesting that *flt4* and *miR-221* act in the same pathway. By contrast, reduction of *miR-221* in mutant embryos bearing a null *kdrl^um19* allele decreased ISV length compared to control *kdrl^um19* mutant embryos (Figures 2E–2G), which normally display variable partial shortening in ISV length (Covassin et al., 2009). The enhanced ISV defect in embryos lacking *miR-221* and *kdrl* is similar to the effect of simultaneously reducing *flt4* and *kdrl* (Covassin et al., 2006b). These observations suggest that *miR-221* acts parallel to *vegfa* and *kdrl* and is likely acting in a common pathway with *vegfc* and *flt4.* Despite this genetic interaction, we did not detect changes in *miR-221* levels in the absence of *flt4* (Figure S2D) and, as noted above, *flt4* levels were normal in *miR-221*-deficient embryos (Figures S2A and S2B).

We next determined if *miR-221* function was required for Vegfc/Flt4 signaling by assessing the response of *miR-221*-deficient embryos to ectopically expressed Vegfc. We used the heat shock 70 (*hsp70*) promoter to inducibly express Vegfc in frame with monomeric red fluorescent protein (mCherry) separated by the viral 2A peptide sequence in zebrafish embryos. Mosaic Vegfc overexpression following heat shock at 15 somite stage caused ectopic branching of ISVs along the horizontal myoseptum in control embryos at 33 hpf (Figures 2H and 2L), but not in *flt4*-deficient embryos (Figures 2I and 2L) indicating that this effect is dependent on the Flt4 receptor. Likewise, *miR-221*-deficient embryos displayed significantly fewer ectopic vessels in response to Vegfc (Figures 2J and 2L). The loss of ectopic sprouting was not generally attributable to partial ISV formation caused by *flt4*- or *miR-221* deficiency, as *kdrl^um19* mutant embryos, which also exhibit partial ISV sprouts (see above), form ectopic vessels in response to Vegfc (Figures 2K and 2L). Together, these results suggest that *miR-221* is required for Vegfc/Flt4 signaling during ISV sprouting.

miR-221 Is Required for Endothelial Tip Cell Proliferation and Migration

In sprouting blood vessels, *flt4* expression is highly dynamic and becomes restricted to endothelial tip cells (Covassin et al., 2006b; Siekmann and Lawson, 2007; Tammela et al., 2008). Since *miR-221* was required for ISV growth and Vegfc/Flt4-induced angiogenesis, we reasoned that it might play a role in governing endothelial tip cell behaviors. To determine if this was the case, we performed two-photon time-lapse microscopy on embryos lacking or overexpressing *miR-221*. In control embryos, ISVs generally formed by migration of endothelial tip cells from the dorsal aorta followed by a second trailing cell (Figure 3A, 19:30 and 20:54; Movie S1), as shown previously (Siekmann and Lawson, 2007). Once reaching the horizontal myoseptum, tip cells in most ISVs divided (Figure 3A, 20:54 to 24:36) and a single daughter cell subsequently migrated dorsally to form the dorsal longitudinal anastomtic vessel (DLAV) (Figure 3A, 27:01).
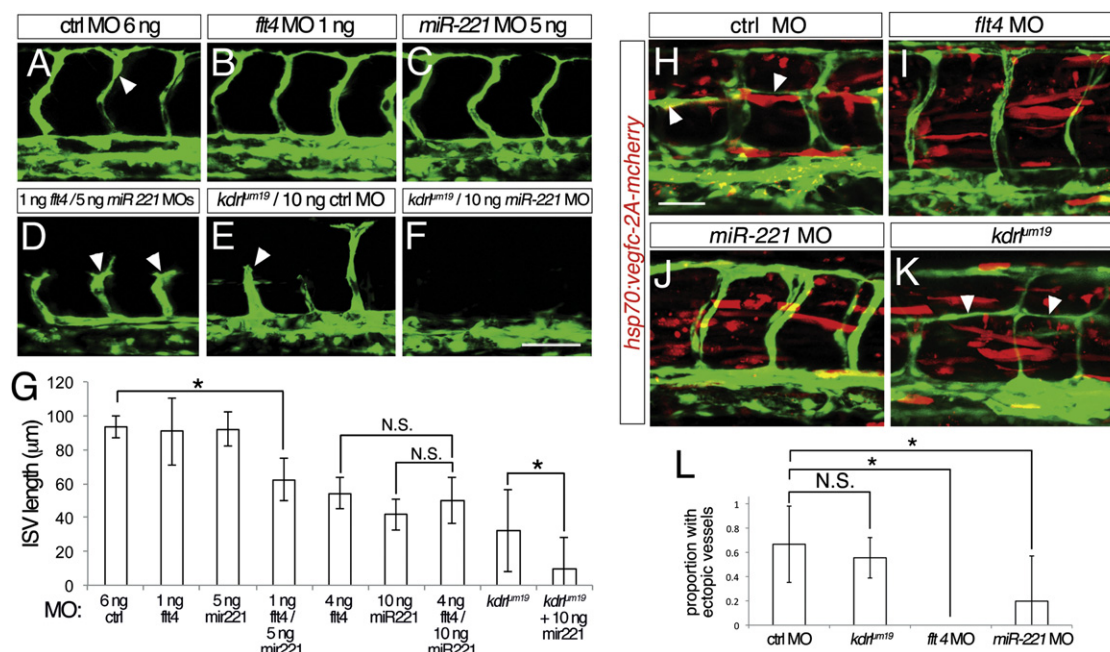
Figure 2. miR-221 Is Required for Vegfc/Flt4 Signaling

(A–F) Confocal micrographs Tg(fli1a:egfp)^{y1} embryos at 27 hpf; arrowheads denote ISVs; lateral views, dorsal is up, anterior to the left. (A) Embryo injected with 6 ng control MO. (B) Embryo injected with 1 ng flt4 and 5 ng control MO. (C) Embryo injected with 1 ng control and 5 ng miR-221 MO. (D) Embryo injected with 1 ng flt4 MO and 5 ng miR-221 MO. (E) kdrl^{um19} mutant embryo injected with 10 ng control MO. (F) kdrl^{um19} mutant embryo injected with 10 ng of miR-221 MO.

(G) Quantification of ISV length in wild-type or kdrl^{um19} mutant embryos injected with indicated MOs. Measurements were made of four adjacent ISVs per embryo in at least 18 embryos from three separate injections; *p < 0.001; N.S., not statistically different.

(H–K) Tg(fli1a:egfp)^{y1} embryos injected with hsp70:vegfc-2A-mcherry transposable element and heat shocked at 15 ss. Red indicates Vegfc-2A-mcherry expression. Arrowheads indicate ectopic formation of vessels. Embryos at 33 hpf coinjected with (H) 10 ng control MO, (I) 2 ng flt4 MO, (J) 10 ng miR-221 MO, or (K) mutant for kdrl^{um19}.

(L) Proportion of hemisegments with ectopic vessel sprouts in embryos injected with 25 pg Tol2-hsp70:vegfc-2A-mcherry and 25 pg Tol2 transposase. Embryos were co-injected with indicated MO, or were mutant for the kdrl^{um19} allele as determined by genotyping following phenotypic analysis. *p < 0.02; N.S., not significant. Scale bars are (A–F) 50 μm and (H–K) 25 μm.

In the absence of miR-221, the initial rate of movement for tip and trailing cells from the dorsal aorta into the ISV was relatively normal (Figure 3B, 19:30 to 20:50; Movie S2; Figure S3A). However, subsequent migration of tip cells from the horizontal myoseptum to the DLAV was significantly slower than in control embryos (for example, compare Figure 3B, 26:51 to Figure 3A, 24:36; Movie S2, Figure S3A). In addition, tip cells often failed to divide in miR-221-deficient embryos (Figure 3B; Movie S2).
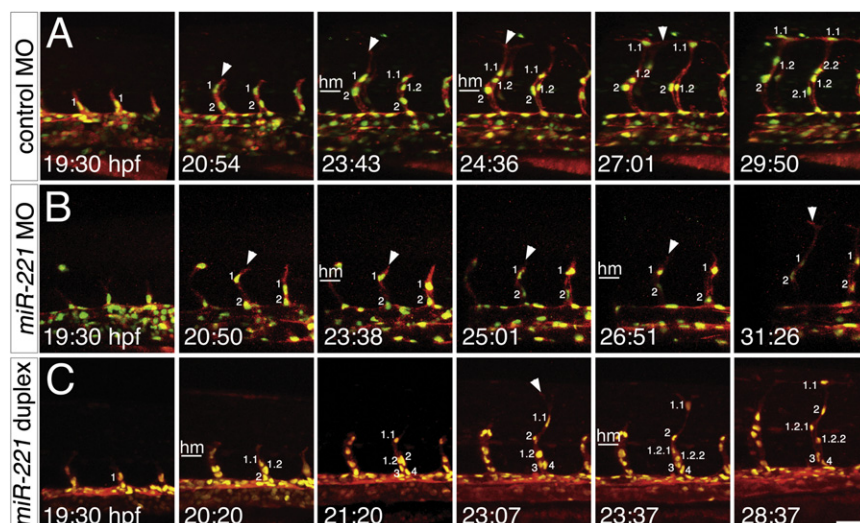

Figure 3. miR-221 Regulates Migration and Proliferation of Tip Cells

(A–C) Still images from time-lapse analysis of (A and B) Tg(fli1a:negfp)^{y7};(kdrl:ras-cherry)^{s916} or Tg(fli1a:negfp)^{y7};(kdrl:tagrfap-caax)^{is19} embryos. Time (hpf) is noted in the bottom left hand corner. Nuclei are numbered; successive numbers indicate new cells that migrated from the dorsal aorta, decimals indicate daughter cells arising from cell division. Lateral views, dorsal is up, anterior to the left. Horizontal white line denotes horizontal myoseptum (hm). (A) Embryo injected with 10 ng control MO. (B) Embryo injected with 10 ng miR-221 MO. (C) Embryo injected with 500 μM miR-221 duplex. Scale bar is 25 μm.
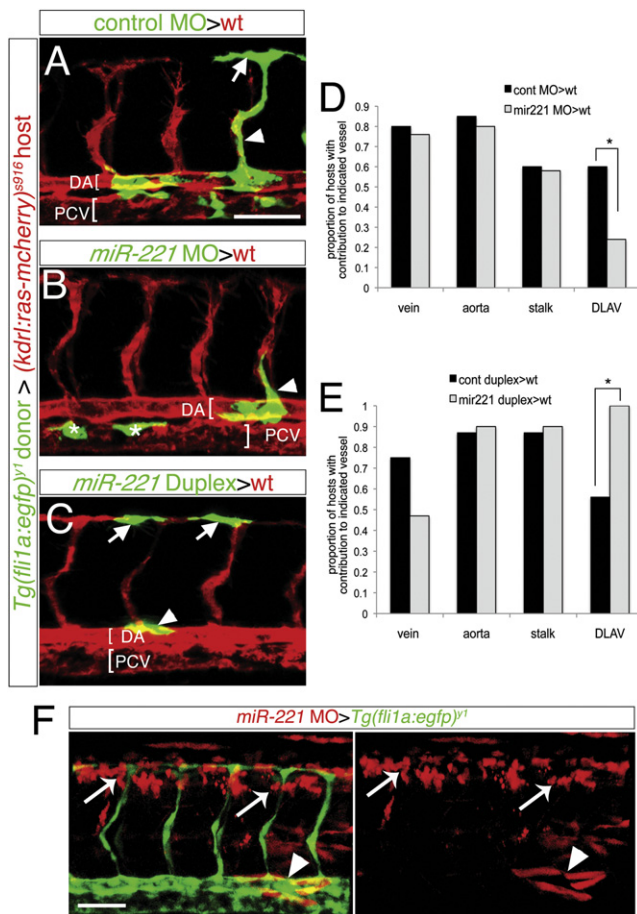See Movies S1, S2, and S3.

Figure 4. *miR-221* Acts Endothelial Cell Autonomously to Drive Tip Cell Potential

(A–C and F) Confocal micrographs of mosaic embryos at 27 hpf following cell transplantation. (A–C) Donor *Tg(fli1a:egfp)^y1* cells are green, host *Tg(kdrl:ras-mcherry)^s916* vessels are red; DA, dorsal aorta; PCV, posterior cardinal vein, both indicated by brackets. (A) Donor control cells in DLAV (arrow) and ISV stalk (arrowhead). (B) Donor *miR-221*-deficient cells in the ISV stalk (arrowhead). Asterisks indicate donor cells in the PCV. (C) Donor cells over-expressing *miR-221* in DLAV (arrows) and dorsal aorta (arrowhead).

(D and E) Proportion of host embryos with donor contribution to indicated blood vessel type. (D) *p = 0.04. (E) *p = 0.001.

(F) *Tg(fli1a:egfp)^y1* host embryo with *miR-221*-deficient donor cells labeled with rhodamine in nonendothelial cell types surrounding the ISVs, including neural tube (white arrows) and somites (white arrowheads). Scale bars are 50 μm.

Together, these defects resulted in delayed formation of the ISV and DLAV, which were ultimately comprised of fewer endothelial cells in *miR-221*-deficient embryos (see below). By contrast, injection of *miR-221* duplex induced precocious division of tip cells prior to reaching the horizontal myoseptum (Figure 3C, 19:30 to 20:20; Movie S3). In addition, excessive numbers of cells from the dorsal aorta continued to migrate into the ISV (Figure 3C, 20:20 to 23:07), further increasing cell numbers in the ISVs (Figure 3C, 28:37 and see below), although ISV growth rate was not faster than in control embryos (data not shown). Consistent with our time-lapse observations, fewer tip cells in *miR-221*-deficient ISVs incorporated BrdU than in control embryos when pulsed beginning at 20 hpf, whereas exogenous

miR-221 expression increased BrdU incorporation in cells that contributed to the DLAV (Figures S3B and S3C). Interestingly, the number of BrdU-positive cells in the dorsal aorta and posterior cardinal vein did not change significantly in either case (Figure S3D), suggesting a preferential effect of *miR-221* on ISV tip cell proliferation. These observations indicate that *miR-221* is required for both migration and proliferation of endothelial tip cells during ISV angiogenesis.

We have previously assessed the potential of an endothelial cell to be a tip cell (referred to hereafter as "tip cell potential") by determining its ability to contribute to the DLAV, which, based on time-lapse analysis, is initially formed from a daughter of the initial ISV tip cell. Using this assay, we have successfully demonstrated that endothelial cells lacking Notch activity, which exhibit excessive proliferation and migration, preferentially localize to the DLAV (Siekmann and Lawson, 2007), whereas recent studies demonstrate a similar behavior for endothelial cells partially deficient in plexin signaling (Zygmunt et al., 2011). To assess the tip cell potential of *miR-221*-deficient or overexpressing cells, and to confirm the endothelial autonomy of these effects, we transplanted donor cells from *Tg(fli1a:egfp)^y1* embryos injected with *miR-221* MO or *miR-221* duplex, respectively, into wild-type *Tg(kdrl:ras-cherry)^s916* host embryos. Control donor cells contributed well to all host blood vessels in the zebrafish trunk (Figures 4A, 4D, and 4E; control MO into WT, n = 20; control duplex into WT, n = 16), whereas *miR-221*-deficient endothelial cells contributed less frequently to the DLAV (Figures 4B and 4D; n = 17), consistent with their reduced proliferation and migratory rates observed in time-lapse analysis (see above). On the contrary, donor cells expressing exogenous *miR-221* showed an enhanced ability to contribute to the DLAV (Figures 4C and 4E; n = 21). Donor cells with either gain or loss of *miR-221* expression otherwise contributed to most other blood vessel positions, ruling out a general defect in endothelial cell specification (Figures 4A–4E). Furthermore, ISV formation was normal in embryos where *miR-221*-deficient donor cells contributed only to surrounding neural tube or somite tissue but not endothelial cells (Figure 4F; n = 10). Thus, *miR-221* increases tip cell potential during ISV angiogenesis and does so in an endothelial autonomous manner.

miR-221 Is Negatively Regulated by Notch Signaling

The defects caused by exogenous *miR-221* were similar to those associated with loss of *dll4* (Hellström et al., 2007; Leslie et al., 2007; Siekmann and Lawson, 2007), suggesting an antagonistic relationship between *miR-221* and Notch signaling. Therefore, we investigated the genetic interaction between *miR-221* and *dll4* by comparing ISV length and cell numbers in embryos following knockdown of one or both of these genes. Similar to previous observations, *dll4* deficiency resulted in significantly more ISV endothelial cells at 27 hpf than in control embryos (Figures 5A, 5B, and 5J), similar to injection of *miR-221* duplex (Figures 5C and 5J). By contrast, *mir-221* knockdown significantly decreased cell numbers, as well as ISV length (Figures 5D, 5J, and 5K), consistent with time-lapse analysis (see Figure 3). Likewise, simultaneous reduction of *mir-221* and *dll4* decreased ISV cell number and length compared to *dll4* knockdown alone (Figures 5E, 5J, and 5K). At 35 hpf, *dll4*-deficient embryos displayed excessive cell numbers compared to control
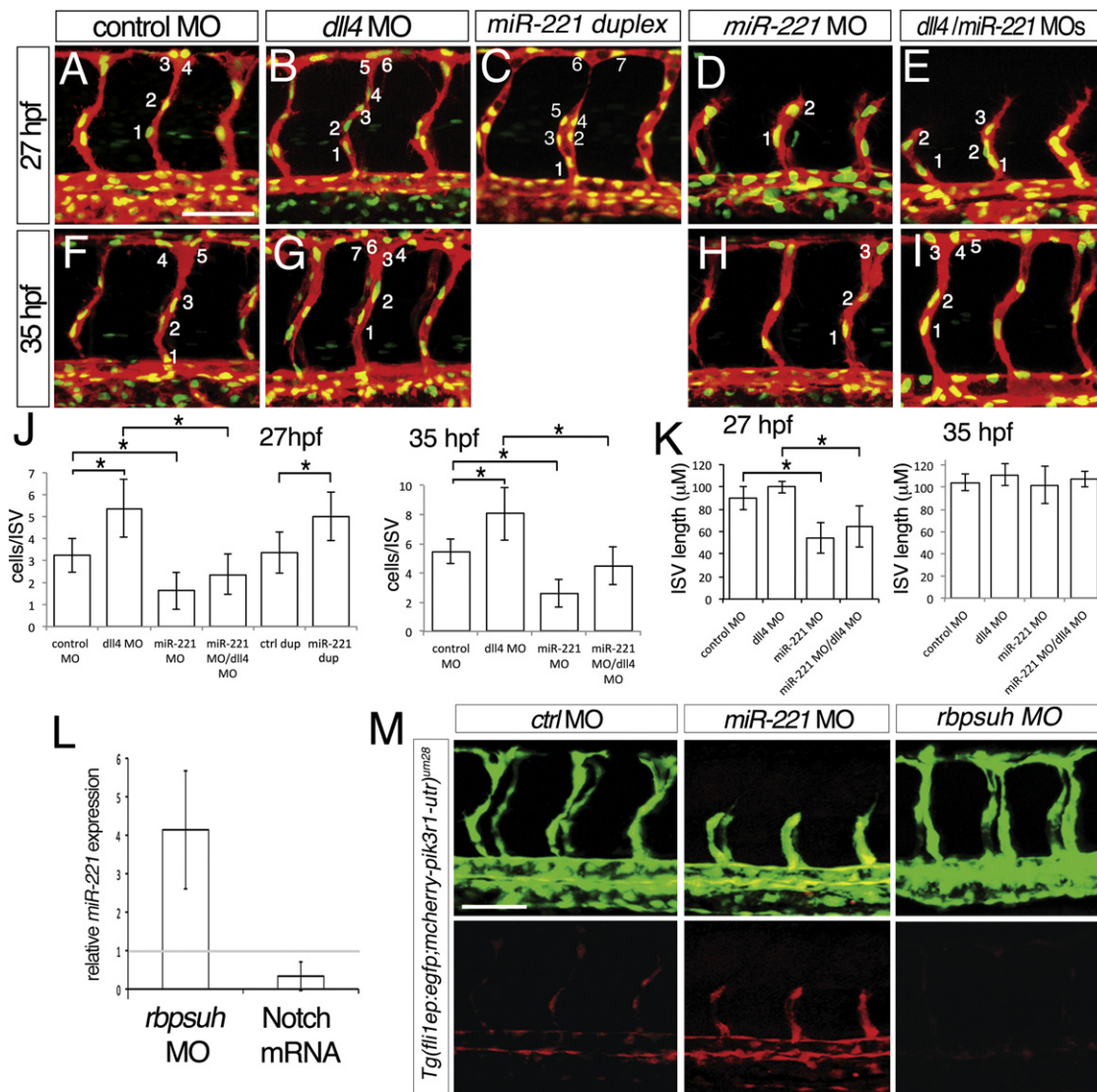
Figure 5. *miR-221* Is Required for the Notch-Deficient "Hyper"-Angiogenesis Phenotype

(A–I), Confocal micrographs of *Tg(fli1a:negfp)^{y7};(kdrl:ras-cherry)^{s916}* embryos, lateral views, dorsal is up, anterior to the left. Numbers indicate nuclei in representative intersegmental blood vessels (ISV). (A–E) Embryos at 27 hr post fertilization (hpf). (F–I) Embryos at 35 hpf. (A and F) Embryos injected with 25 ng of control MO. (B and G) Embryos injected with 15 ng of *dll4* MO. (C) Embryo injected with 500 μM *miR-221* duplex. (D and H) Embryo injected with 10 ng of miR-221 MO. (E and I) Embryos coinjected with 15 ng of *dll4* MO and 10 ng of *miR-221* MO.

(J and K) (J) Quantification of endothelial number and (K) ISV length in *Tg(fli1:ngfp)^{y7};(kdrl:ras-cherry)^{s916}* embryos injected with indicated MO(s); *p < 0.0001. Measurements were determined for four adjacent ISVs per embryo in at least eight embryos from three separate injections.

(L) Fold change of mature *miR-221* levels assessed by qRT-PCR in embryos injected with 2.5 ng *rbpsuh* MO or with mRNA encoding an activated form of Notch compared to control embryos.

(M) Confocal micrographs of *Tg(fli1ep;mcherry-pik3r1-utr)^{um28}* embryos injected with 10 ng control MO, 10 ng *miR-221* MO, or 2.5 ng Rbpsuh MO. Lateral views, dorsal is up, anterior to the left. Scale bars are 50 μm.

embryos (Figures 5F, 5G, and 5J), whereas ISVs in *mir-221*-deficient embryos, which have recovered to form a DLAV and exhibit normal ISV length (Figures 5K and 5H), displayed fewer ISV cells (Figures 5H and 5J). Furthermore, *dll4*-deficient embryos lacking *miR-221* displayed normalized numbers of cells similar to wild-type ISVs (Figures 5I and 5J). Taken with our finding that exogenous *miR-221* drives excessive migration and proliferation, these observations suggest that *miR-221* is required for excessive angiogenesis associated with loss of Notch.

Notch signaling blocks angiogenesis, in part, by repressing *flt4* expression (Siekmann and Lawson, 2007). Since *miR-221* acted in the *flt4* signaling pathway, we determined whether it might also be repressed by Notch. In embryos injected with a MO targeting the Rbpsuh DNA binding protein, which is required for Notch signaling (Bailey and Posakony, 1995; Fortini and Artavanis-Tsakonas, 1994), we found that *miR-221* is upregulated (Figure 5L). By contrast, injection of mRNA encoding an activated form of Notch repressed *miR-221* levels when
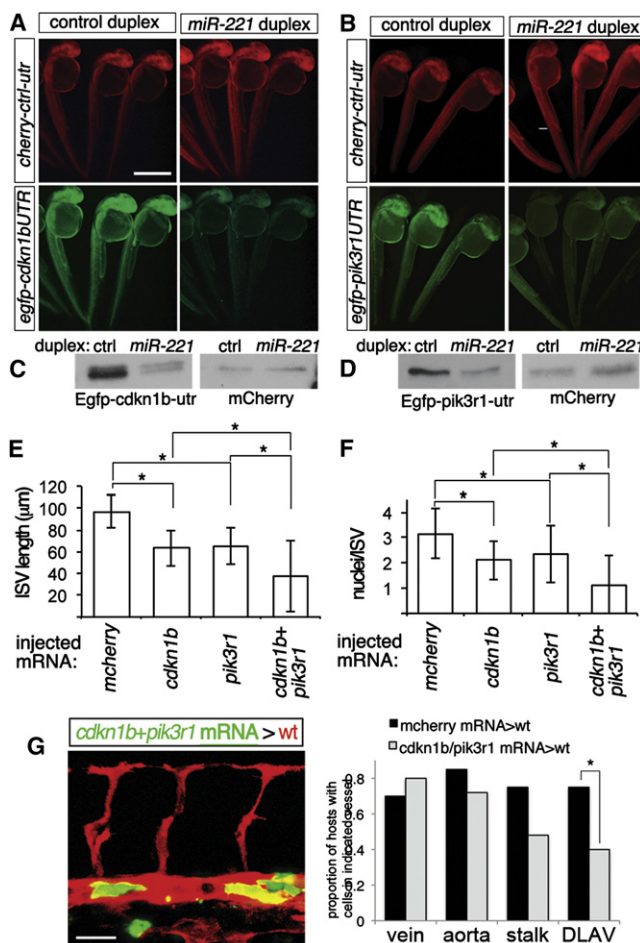
Figure 6. *cdkn1b* and *pik3r1* Are Targets of *miR-221*

(A and B) Fluorescent images of embryos co-injected with 150 pg each of *mcherry* mRNA fused to control 3′ UTR and *egfp* mRNA fused to (A) *cdkn1b* 3′ UTR or (B) *pik3r1* 3′ UTR with 100 μM indicated duplex RNA. Lateral views, dorsal is up, anterior to the left. Scale bar is 500 μm.

(C and D) Western analysis of embryos in (A) and (B).

(E and F) (E) ISV length and (F) cell number in *Tg(fli1:egfp)^y1* and *Tg(fli1:negfp)^y7* embryos, respectively, at 27 hpf injected with 500 pg of indicated mRNAs. For coinjections, 200 pg of *cherry2A-cdkn1b* and 300 pg *cherry2A-pik3r1* mRNA were used. *p < 0.002.

(G) *Left*, host *Tg(kdrl:ras-mcherry)^s916* embryo at 27 hpf following transplantation of cells from a *Tg(fli1a:egfp)^y1* embryo injected with 200 pg *cdkn1b* and 300 pg *pik3r1* mRNA *Right*, proportion of embryos displaying donor cells in indicated vessel type. Control donor cells were from embryos injected with 500 pg *mcherry* mRNA. *p = 0.03. Scale bar is 25 μm.

compared to control injected embryos (Figure 5L). To demonstrate that the effect of Notch signaling on *miR-221* levels was occurring in endothelial cells, we utilized an endothelial autonomous microRNA sensor assay (Nicoli et al., 2010). In this case, we generated a transgenic line (*Tg(fli1ep:egfp;mcherry-pik3r1)^um28*) using an endothelial cell-specific bicistronic vector driving *mcherry* fused to a 3′ UTR containing two *miR-221* binding sites (Figure S4A and see below) and *egfp* fused to a control 3′ UTR. *Tg(fli1ep:egfp;mcherry-pik3r1-utr)^um28* embryos exhibited robust green fluorescence in trunk blood vessels at 28 hpf, whereas *mcherry* levels appeared lower (Fig-

ure 5M). Consistent with *miR-221*-mediated repression of the *mcherry* transcript, we observed increased red fluorescence in *Tg(fli1ep:egfp;mcherry-pik3r1)^um28* embryos injected with *miR-221* MO (Figure 5M; Figure S4B). By contrast, Mcherry expression was significantly repressed following injection of *rbpsuh* MO (Figure 5M; Figure S4B), consistent with our observation that *miR-221* levels are increased in Notch-deficient embryos (Figure 5L). Similar results were observed with a second 3′ UTR bearing *miR-221* sites (see below and Figures S4B and S4C). Taken together, our results demonstrate that Notch negatively regulates *miR-221* to block endothelial tip cell proliferation and migration.

Repression of Two Distinct Targets by *miR-221* Is Required for Angiogenesis

In tumor cells *miR-221* drives proliferation by repressing *cyclin dependent kinase inhibitor 1b* (*cdkn1b*; Galardi et al., 2007), which blocks cell cycle progression. Since our studies demonstrated a block in endothelial proliferation in *miR-221*-deficient embryos, *cdkn1b* was a viable candidate target during angiogenesis. In addition, we identified *pik3r1*, the p85-alpha regulatory subunit of the phosphoinositide-3-kinase (PI3K) complex, as a candidate target of *miR-221*. Given the importance of PI3K signaling in vascular development (Graupera et al., 2008), we reasoned that this transcript was also a possible functional target of *miR-221* during ISV angiogenesis.

Both *cdkn1b* and *pik3r1* 3′ UTRs contain *miR-221* binding sites (Figure S4A; data not shown) and were repressed by *miR-221* in whole-embryo reporter assays (Figures 6A–6D) and endothelial cells in vivo (Figure 5M; Figures S4B and S4C). We also detected low-level expression of both transcripts in the trunk blood vessels and isolated *kdrl:egfp* cells (Figures S5A and S5B). Consistent with the possibility that increased levels of *cdkn1b* and *pik3r1* contributed to defects associated with loss of *miR-221* (see above), overexpression of *cdkn1b* or *pik3r1*, or both together, reduced ISV length and cell numbers (Figures 6E and 6F), without an overt effect on general development (Figure S5C). Furthermore, mosaic analysis demonstrated that cells expressing both *pik3r1* and *cdkn1b* contribute less frequently to the tip cell position than control (Figure 6G; control mRNA > WT, n = 20, *cdkn1b/pik3r1* mRNA > WT, n = 25), similar to *miR-221*-deficient cells (Figures 4B and 4D). These results indicate that increased levels of *cdkn1b* and *pik3r1* can negatively affect tip cell potential in an endothelial autonomous manner, further supporting that they are normally targeted by *miR-221* during ISV sprouting.

Our results suggest that *miR-221* controls ISV growth by inducing proliferation and PI3K activity through repression of *cdkn1b* and *pik3r1*, respectively. To further investigate the importance of proliferation and PI3K during ISV growth, we treated embryos at 20 hpf with either 5-hydroxyurea and aphidocolin (HUA/AP) to block cell cycle or LY294002 to inhibit PI3K. In both cases, we observed a significant decrease in ISV length and cell number (Figures 7A–7C), although embryos were normal and did not exhibit changes in *vegfa* or *kdrl* expression (Figure S5D; data not shown). The decrease in ISV cell number was more modest in LY294002-treated embryos than those treated with HUA/AP (Figure 7C). Furthermore, similar to *miR-221* knockdown, HUA/AP prevented BrdU incorporation into ISV tip cells,
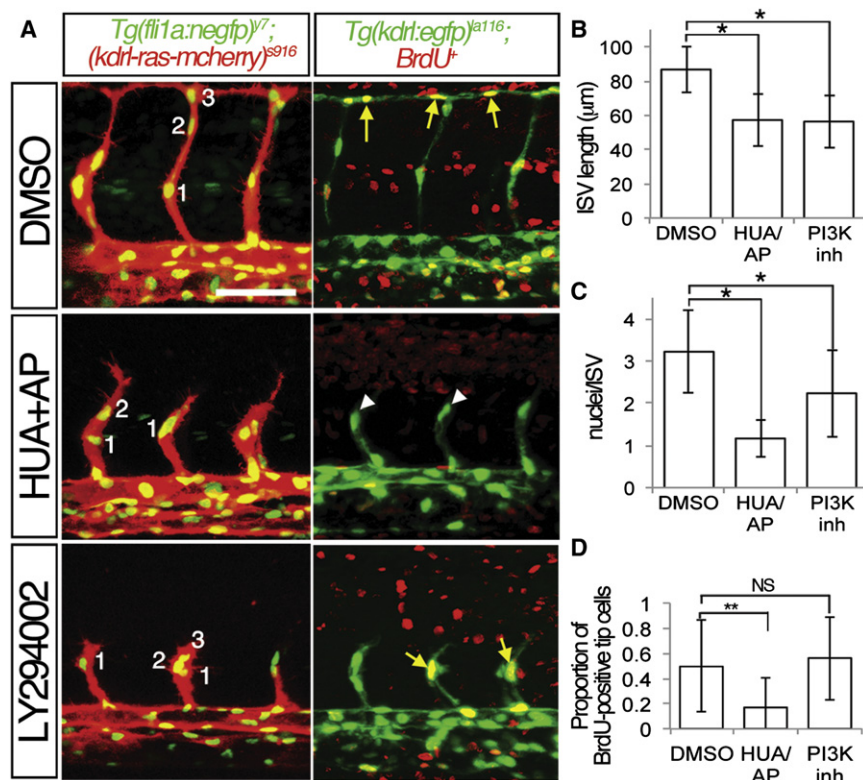
Figure 7. Proliferation and PI3K Are Required for ISV Growth

(A) Embryos at 27 hpf treated with 4% DMSO, 150 μM 5-hydroxyurea, and 20 mM aphidocolin (HUA/AP), or 25 μM LY294002 (PI3K inh) beginning at 20 hpf. *Left panels*, confocal micrographs of *Tg(fli1:negfp)*[y7]*;(kdrl:ras-cherry)*[s916] embryos. (right panels) Two-photon micrographs of *Tg(kdrl:egfp)*[la116] embryos pulsed with BrdU at 20 hpf. Lateral views, dorsal is up, anterior to the left, yellow arrows denote BrdU-positive endothelial nuclei; BrdU-negative endothelial nuclei indicated by white arrowheads. Scale bar is 50 μm.

(B and C) Quantification of (B) ISV length in microns and (C) number of nuclei per ISV in *Tg(fli1:negfp)*[y7]*;(kdrl:ras-cherry)*[s916] embryos at 27 hpf treated as in (A). *p < 0.0001.

(D) Quantification of BrdU-positive DLAV or ISV tip cells in *Tg(kdrl:egfp)*[la116] embryos at 27 hpf treated as in (A). **p < 0.02. NS, not significant.

whereas LY294002 did not (Figures 7A and 7D), suggesting that PI3K inhibition does not affect endothelial cell proliferation during sprouting. Our results demonstrate that *pik3r1* overexpression and PI3K inhibition similarly blocked ISV growth, suggesting that increased *pik3r1* in the absence of *miR-221* blunts PI3K signaling output. To determine if this was the case, we generated transgenic zebrafish (referred to as *Tg(fli1ep:phaktegfp-2A-mcherry)*[um63]) bearing EGFP fused to the pleckstrin homology domain of human Akt1 (PH-AKT-EGFP), which localizes to the membrane in response to PI3K activation (Astoul et al., 1999), and a coexpressed red fluorescent protein. In *Tg(fli1ep:phaktegfp-2A-mcherry)*[um63] embryos lacking *miR-221*, we observed decreased filopodial localization of PH-AKT-EFP compared to control (Figures S5E and S5F). Furthermore, partial reduction of *pik3r1* to levels that do not affect ISV formation (see below) restores filopodial PH-AKT-EGFP localization in *miR-221*-deficient *Tg(fli1ep:phaktegfp-2A-mcherry)*[um63] embryos (Figures S5E and S5F). These observations suggest that increased levels of *pik3r1* in the absence of *miR-221* cause reduced or mislocalized PI3K output in sprouting endothelial cells, which contributes to the observed defects in ISV growth.

Our results suggested that upregulation of *pik3r1* and *cdkn1b* is the likely cause of ISV growth defects in *miR-221*-deficient embryos. If this were the case, then reducing their levels would rescue the phenotypes in *miR-221*-deficient embryos. To investigate this possibility, we injected embryos with MOs to inhibit splicing of *cdkn1b* or *pik3r1* (Figures S6A–S6D). In all cases, we coinjected *tp53* MO to eliminate off-target toxicity. Reduction of *tp53* alone did not rescue defects associated with *miR-221* deficiency (Figures 8A, 8E, 8J, and 8L). Wild-type embryos lack-

ing *cdkn1b* exhibited excessive numbers of ISV endothelial cells (Figures 8A, 8B, and 8I), similar to embryos injected with *miR-221* duplex (see Figures 5C and 5J), but were otherwise normal (Figure S6D). Embryos injected with 10 ng of MO to reduce *pik3r1* levels displayed variable shortening of ISV length and a slight, but nonsignificant decrease in ISV cell numbers and were otherwise overtly normal (Figures 8C, 8I, and 8K; Figures S6B–S6D). Injection of 5 ng *pik3r1* MO did not cause a phenotype (Figures 8D, 8I, and 8K). We attempted to rescue *miR-221* deficiency by coinjecting 5 ng of either *cdkn1b* or *pik3r1* MO with 10 ng of *miR-221* MO. In both cases, we observed a partial restoration of ISV length, although not to control levels (Figures 8E–8G and 8L). Interestingly, knockdown of *cdkn1b*, but not *pik3r1*, restored ISV endothelial cell number to control levels in the absence of *miR-221* (Figure 8J), consistent with the differential effects of HUA/AP and LY294002 on endothelial proliferation and ISV growth noted above. Simultaneous knockdown of *ckdn1b* and *pik3r1* in *miR-221*-deficient embryos fully restored both ISV length and cell number (Figures 8H, 8J, and 8L), indicating that these two targets together mediated the function of *miR-221* during ISV growth. Furthermore, endothelial cells with reduced levels of *cdkn1b* and *pik3r1* localized to the DLAV at a greater frequency than control cells in mosaic embryos (Figure 8M; control MO data are same as those shown in Figure 4; *cdkn1b/pik3r1* MO > WT, n = 24), similar to cells expressing exogenous levels of *miR-221* (see Figure 4E). Thus, *miR-221* induces tip cell proliferation through downregulation of *cdkn1b* and promotes optimal PI3K output by reducing *pik3r1*. Together, these effects contribute to endothelial tip cell migration and proliferation during angiogenesis.

DISCUSSION

The ability of an endothelial cell to dynamically respond to proangiogenic cues is essential to coordinate distinct cellular
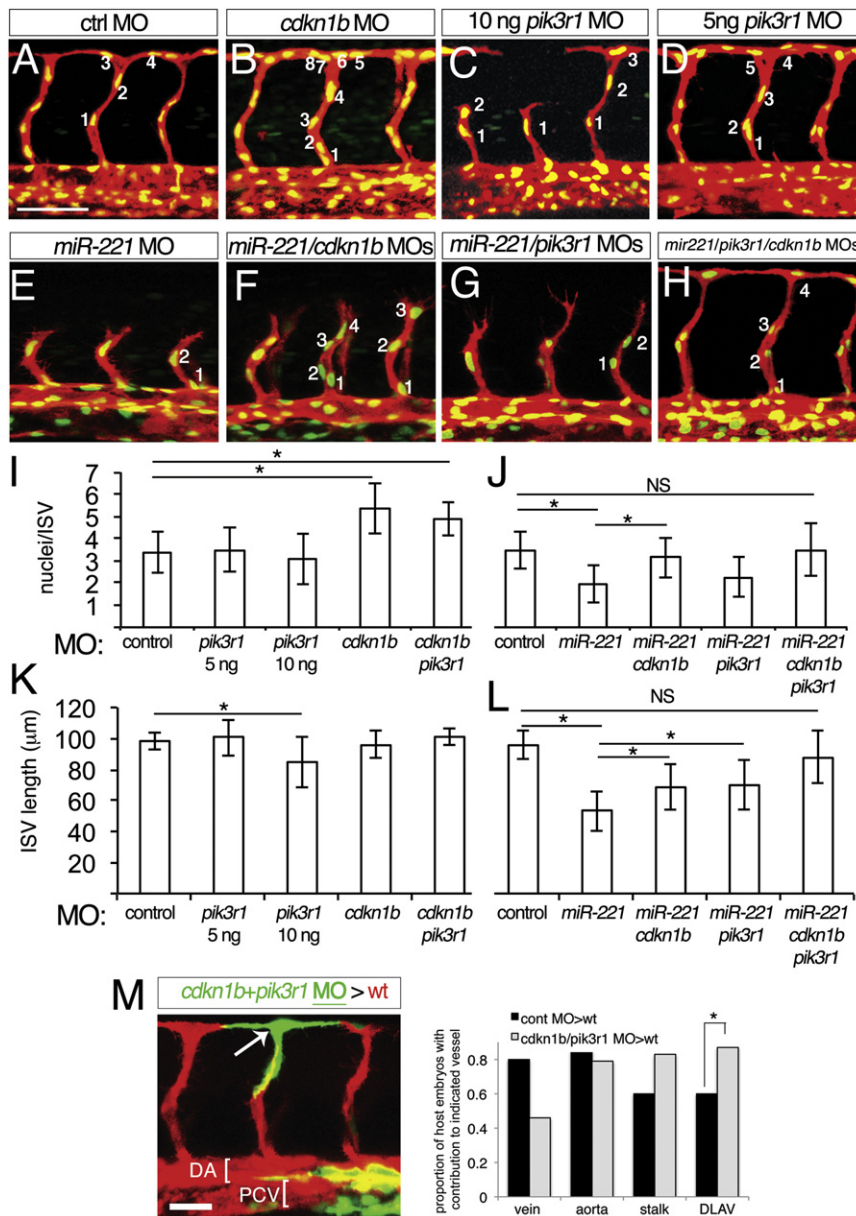
Figure 8. *pik3r1* and *cdkn1b* Are Functional Downstream Targets of miR-221

(A–H) *Tg(fli1a:negfp)^{y7};(kdrl:ras-cherry)^{s916}* embryos at 27 hpf. Numbers denote cell nuclei of representative ISV. All embryos were co-injected with 1 ng of *p53* MO. Scale bar is 50 μm. Embryo injected with (A) 15 ng control MO (B) 5 ng *cdkn1b* MO, (C) 10 ng *pik3r1* MO, (D) 5 ng *pik3r1* MO, (E) 10 ng *miR-221* MO, (F) 10 ng *miR-221* and 5 ng *cdkn1b* MOs, (G) 10 ng *miR-221* and 5 ng *cdkn1b* MOs, and (H) 10 ng miR-221, 3 ng *cdkn1b*, and 3 ng *pik3r1* MOs.

(I–L) (I and J) Quantification of cells per ISV and (K, L) ISV length in embryos at 27 hpf injected with MOs as above, except control MO, which was injected at (I and K) 10 ng and (J and L) 15 ng doses. *p < 0.001; N.S., not significant. Measurements were obtained from four adjacent ISVs in at least ten embryos from three separate experiments. (M) *Left*, host *Tg(kdrl:ras-mcherry)^{s916}* embryo at 27 hpf following transplantation of cells from a *Tg(fli1a:egfp)^{y1}* embryo injected with 3 ng *cdkn1b* MO and 5 ng *pik3r1* MO. *Right*, proportion of embryos displaying donor cells in indicated vessel type. Data from control donor cells is the same as in Figure 4D. *p = 0.07. Scale bar is 25 μm.

appeared normal following loss of *miR-221*, *pik3r1*, or PI3K signaling and *tp53* knockdown did not rescue *miR-221* deficiency. Instead, we believe that *pik3r1* is important for tip cell migration, consistent with the role for the PI3K catalytic p110α subunit in endothelial cells (Graupera et al., 2008). Our results further suggest that *miR-221* appropriately tunes PI3K signaling output by controlling the levels of a PI3K regulatory subunit. Pik3r1 usually exists in a 1:1 ratio with a catalytic subunit of the PI3K signaling complex (Geering et al., 2007), such as p110α, and both proteins are otherwise unstable (Yu et al., 1998). Pik3r1 inhibits the catalytic subunits, but is also required for PI3K activity following membrane localization of the Pik3r1/p110 complex and activation by a receptor tyrosine kinase (Vanhaesebroeck et al., 2010). A central question is how increased Pik3r1 may alter PI3K signaling to block sprouting. In some contexts, Pik3r1 acts independently of PI3K catalytic subunits (García et al., 2006), suggesting that increased Pik3r1 may interfere with other signaling pathways required for angiogenesis. However, in this case excess Pik3r1 would not affect PI3K output, yet we observe decreased PI3K activity in the filopodia of *miR-221*-deficient ISVs. A more likely possibility is that increased Pik3r1 alters the appropriate balance in regulatory and catalytic subunits, which can be composed of several different isoforms that are present in endothelial cells (Graupera et al., 2008). In turn, a shift in stoichiometry may squelch receptor tyrosine kinase signaling output and PI3K activity. It is also possible that these changes lead to

behaviors with its neighbors. Without this coordination, productive angiogenesis is hindered. Our present work provides evidence that posttranscriptional regulation by microRNAs plays an important role in this process. In particular, we identify *miR-221* as an essential regulator of angiogenesis in embryonic zebrafish and provide evidence that supports a role for *miR-221* in endothelial tip cell proliferation and migration.

miR-221 appears to act in sprouting endothelial cells through repression of two distinct target transcripts: *pik3r1* and *cdkn1b*. Our results suggest that these target genes control distinct tip cell behaviors. Although *miR-221*-mediated downregulation of *cdkn1b* was required for proliferation, PI3K signaling was dispensable for this behavior in tip cells. Although repression of *pik3r1* by microRNAs in other contexts can cause p53-dependent apoptosis (Park et al., 2009), endothelial tip cell survival

inappropriate subcellular localization of PI3K complexes. In this regard, it is of note that PI3K signaling is active in endothelial filopodia in developing ISVs. Increased Pik3r1 may alter the subcellular localization of PI3K complexes, thereby reducing filopodia PI3K activity, possibly without a change in total cellular PI3K output. In any event, microRNA regulation of PI3K signaling appears to be an emerging theme in the control of this crucial signaling regulator as *miR-126* similarly regulates Vegfr-2 signaling output through modulation of Pik3r2 (Fish et al., 2008; Wang et al., 2008).

The importance of *miR-221* for endothelial tip cell migration and proliferation is consistent with its requirement for signaling through *flt4*. Interestingly, neither *vegfc*, nor *flt4* expression is regulated by *miR-221*, whereas *miR-221* expression is normal in *flt4*-deficient embryos. We believe that the central point of interaction between *miR-221* and *flt4* is at the level of *pik3r1* regulation. Pik3r1 possesses SH2 domains to facilitate interaction with activated receptor tyrosine kinases and is known to interact with Flt4 following binding to Vegfc (Wang et al., 2004). Thus, *miR-221* may directly affect Flt4 signaling output through its regulation of *pik3r1* levels. Although *miR-221* expression is independent of *flt4* itself, we find that it is repressed by Notch activation, similar to *flt4*. Together, our findings suggest a model in which *miR-221* promotes migration and proliferation by potentiating *flt4* signaling through regulation of *pik3r1*, while repressing *cdkn1b*. By contrast, Notch activation in stalk cells represses both *flt4* and *miR-221*. Subsequently, *cdkn1b* levels increase to limit proliferation, whereas an increase in *pik3r1* serves to dampen, or qualitatively shift PI3K output.

In contrast to our findings, exogenous *miR-221* is anti-angiogenic in human venous or lymphatic endothelial cells (Chen et al., 2010; Poliseno et al., 2006; Wu et al., 2011). These effects were mediated through numerous distinct targets depending on the study and included the ETS1 transcription factor (Zhu et al., 2011), the stem cell factor receptor C-KIT (Poliseno et al., 2006), and the transcriptional repressor ZEB2 (Chen et al., 2010). *miR-221* can also increase lymphocyte adhesion through repression of ETS1, leading to a decrease in angiotensin II expression (Zhu et al., 2011). Interestingly, this latter work did not note a migration defect in response to *miR-221* overexpression, as cited in other studies. A possible explanation for these discrepancies is that *miR-221* levels vary significantly in response to both serum and Vegfa (Chen et al., 2010; Suárez et al., 2008), suggesting that growth conditions influence microRNA function in cultured cells. These observations raise the possibility that *miR-221* governs context-specific changes in endothelial behavior depending on cell type or developmental stage. Thus, whereas *miR-221* is an important proangiogenic signal during embryonic development, it may play different roles in the mature circulatory system.

Although *miR-221* is only modestly enriched in endothelial cells and is present at high levels in nonendothelial cell types, *miR-221* deficiency caused remarkably specific developmental vascular defects. There may several reasons for this observation. First, MOs only provide partial knockdown and the observed phenotypes may be manifest only in cell types (e.g., endothelial tip cells) where high gene dosage is required. Second, *miR-221*-deficient embryos may display subtle defects in other tissues and developmental processes. Indeed, the observed vascular defects were only obvious when using a transgenic background to visualize blood vessel morphology. Thus, more careful molecular and cellular analysis applied to other organ systems may reveal further defects associated with *miR-221* reduction. Finally, microRNAs play an important regulatory role by tuning gene expression to appropriate levels. As such, single microRNA deficiency often has very subtle effects on animal development. In this regard our findings are consistent with those in other models. Interestingly, we also noted specific cardiovascular defects associated with knockdown of other microRNAs (e.g., *miR-107* and *miR-20b*), suggesting a widespread role for small RNAs in vascular development. Further screening of microRNA function in zebrafish will likely reveal additional roles for small RNAs in vascular formation, function, and homeostasis.

EXPERIMENTAL PROCEDURES

Zebrafish Lines
Zebrafish used in this study are described in Supplemental Experimental Procedures.

miRNA Library Preparation, Deep Sequencing, and Analysis
Endothelial cells were isolated from $Tg(kdrl:egfp)^{la116}$ embryos as previously (Covassin et al., 2006a). Small RNA (18–24 nt) purification, adaptor ligation, cDNA synthesis and library amplification were performed as described (Gu et al., 2009). Deep sequencing was performed at the Center for AIDS Research at UMass Medical School. Reads were mapped to known zebrafish microRNAs using the latest version of mirDeep (Friedländer et al., 2008).

Northern Blot Analysis, In Situ Hybridization, and Quantitative PCR
For Northern analysis, 5–10 μg of total RNA was resolved on a 15% acrylamide/7 M urea gel and transferred by electrophoresis to positively charged nylon membrane (Millipore) using a Trans-Blot SD apparatus (Bio-Rad). Hybridization and detection using digoxigenin-labeled locked nucleic acid (LNA) probes (Exiqon) were performed as described (Kloosterman et al., 2006). Whole-mount in situ hybridization using LNA or antisense RNA probes was performed as previously (Kloosterman et al., 2006; Nicoli et al., 2010). miRNA-quantitative-PCR was performed using the miScript PCR system (QIAGEN). Probe and primer sequences can be found in the Supplemental Experimental Procedures.

Morpholino and mRNA Injections
MO sequences and primers designed for RT-PCR validation are described in Supplemental Experimental Procedures. Knockdown of the zebrafish *cdkn1b* and *pik3r1* genes was accomplished using MOs targeting splice junctions within these genes that were validated by RT-PCR and qRT-PCR on RNA isolated from injected embryos. MOs targeting *rbpsuh*, *flt4* and *dll4* are described elsewhere (Covassin et al., 2006b; Siekmann and Lawson, 2007). MOs were synthesized by Gene Tools, LLC and dissolved in DEPC water.

MicroRNA Sensor Assays
Whole-embryo and endothelial autonomous microRNA sensor assays were carried out as previously described (Nicoli et al., 2010). For details see Supplemental Experimental Procedures.

Western Blot
Ten to twenty embryos injected with 3′ UTR sensor and control mRNAs at 24 hpf were dechorionated and triturated in calcium free ringer solution (Covassin et al., 2006a) and lysed as described (Rand et al., 2004). Total protein (40 μg) was separated on a 12% SDS-PAGE gel. Western blotting was performed according to standard protocols. GFP and Cherry were sequentially detected using rabbit anti-GFP (1:1,000, Invitrogen) and rabbit anti-DsRed (1:1,000, Clontech), respectively, followed by chemiluminscent immunodetection using anti-rabbit HRP conjugate (1:20,000, Invitrogen).

Chemical Treatments, BrdU Incorporation, and Immunohistochemistry

To block cell division, we treated embryos simultaneously with 150 μM aphidi-colin (Sigma) and 20 mM hydroxyurea (Sigma) as described (Lyons et al., 2005). To block PI3K signaling we used 25 μM LY294002 (Sigma). Drug treatments were performed at 20 hpf on dechorionated embryos in agarose-coated dishes. BrdU labeling was performed by injection of 50 mM *BrdU* in 0.2 M KCl directly into the yolk of Tg(kdrl:egfp)[la116] embryos. Embryos were injected at 20 hpf, transferred to embryo media, and incubated at 28.5°C until 28 hpf. For whole-mount immunostaining, embryos were fixed in 4% paraformalde-hyde for 2 hr at room temperature and transferred to methanol overnight at −20°C. Embryos were rehydrated to PBST (PBS + 0.5% Triton X-100) and incubated in 2N HCl for 1 hr at room temperature, washed in PBST and placed in blocking solution (PBST + 1% DMSO + 1% BSA + 0.2% goat serum) for 30 min at room temperature. To detect BrdU, embryos were immuno-stained with Alexa-594 anti-BrdU antibody (1:200, Invitrogen) and Alexa-488 anti-GFP antibody (1:300, Invitrogen).

Image Acquisition and Vessel Measurements

Whole-mount live and fixed embryos were analyzed using a MZFLIII micro-scope equipped with epifluorescence. Digital images were captured using a Zeiss mRC digital camera and AxioVision software. Confocal stacks in green (excitation 488 nm laser) and red (excitation 651 nm laser) channels were acquired sequentially using a Leica SP2 confocal microscope. Two-photon imaging was performed using a LSM7 MP Laser scanning microscope (Zeiss) equipped with a Chameleon Ti:Sapphire pulsed laser (Coherent, Inc.) and images acquired using ZEN 2009 software. For detection of BrdU and Egfp in *Tg(kdrl:egfp)*[la116] embryos, we sequentially scanned embryos at 1,040 nm (70% power) and 920 nm (20% power). Measurements of ISVs were made straight from the edge of the aorta to the leading edge of the sprout. Two-dimensional projections were generated using Imaris (Bitplane). Except where otherwise indicated, all pairwise comparisons were analyzed for significance using a Student's two-tailed t test. Error bars in all graphs represent SD.

Mosaic Analysis

Transplantations were performed as described (Covassin et al., 2009). Donors were injected with 10 ng of control MO or *miR-221* MO to assess loss-of-func-tion effects or 500 μM of *miR-221* duplex or control duplex to assess gain-of-function effects. The contribution of donor cells was assigned as a percentage of total number of host embryos that display GFP endothelial cells in the indi-cated vessels. To assess nonautonomous effects, donor cells were injected with miniRuby (Invitrogen) and transplanted into *Tg(fli1a:egfp)*[y1] embryos. To determine cell autonomous function of *pik3r1* and *cdkn1b*, donor embryos were coinjected with 5 ng of *cdkn1b* and 5 ng of *pik3r1* MOs or 200 pg of *cdkn1b* and 300 pg of *pik3r1* mRNA, respectively. Control transplants were performed using donors injected with 500 pg *mcherry* mRNA. The proportions of embryos exhibiting contribution to each vessel type following the indicated experimental manipulations were compared using Fisher's exact test.

ACCESSION NUMBERS

The Gene Expression Omnibus accession number for the deep sequencing data reported in this paper is GSE35078.

SUPPLEMENTAL INFORMATION

Supplemental Information includes six figures, Supplemental Experimental Procedures, one table, and three movies and can be found with this article online at doi:10.1016/j.devcel.2012.01.008.

REFERENCES

Astoul, E., Watton, S., and Cantrell, D. (1999). The dynamics of protein kinase B regulation during B cell antigen receptor engagement. J. Cell Biol. *145*, 1511–1520.

Bailey, A.M., and Posakony, J.W. (1995). Suppressor of hairless directly acti-vates transcription of enhancer of split complex genes in response to Notch receptor activity. Genes Dev. *9*, 2609–2622.

Bernstein, E., Caudy, A.A., Hammond, S.M., and Hannon, G.J. (2001). Role for a bidentate ribonuclease in the initiation step of RNA interference. Nature *409*, 363–366.

Bertrand, J.Y., Chi, N.C., Santoso, B., Teng, S., Stainier, D.Y., and Traver, D. (2010). Haematopoietic stem cells derive directly from aortic endothelium during development. Nature *464*, 108–111.

Chen, Y., Banda, M., Speyer, C.L., Smith, J.S., Rabson, A.B., and Gorski, D.H. (2010). Regulation of the expression and activity of the antiangiogenic homeobox gene GAX/MEOX2 by ZEB2 and microRNA-221. Mol. Cell. Biol. *30*, 3902–3913.

Covassin, L., Amigo, J.D., Suzuki, K., Teplyuk, V., Straubhaar, J., and Lawson, N.D. (2006a). Global analysis of hematopoietic and vascular endothelial gene expression by tissue specific microarray profiling in zebrafish. Dev. Biol. *299*, 551–562.

Covassin, L.D., Villefranc, J.A., Kacergis, M.C., Weinstein, B.M., and Lawson, N.D. (2006b). Distinct genetic interactions between multiple Vegf receptors are required for development of different blood vessel types in zebrafish. Proc. Natl. Acad. Sci. USA *103*, 6554–6559.

Covassin, L.D., Siekmann, A.F., Kacergis, M.C., Laver, E., Moore, J.C., Villefranc, J.A., Weinstein, B.M., and Lawson, N.D. (2009). A genetic screen for vascular mutants in zebrafish reveals dynamic roles for Vegf/Plcg1 signaling during artery development. Dev. Biol. *329*, 212–226.

Czech, B., and Hannon, G.J. (2011). Small RNA sorting: matchmaking for Argonautes. Nat. Rev. Genet. *12*, 19–31.

Fish, J.E., Santoro, M.M., Morton, S.U., Yu, S., Yeh, R.F., Wythe, J.D., Ivey, K.N., Bruneau, B.G., Stainier, D.Y., and Srivastava, D. (2008). miR-126 regu-lates angiogenic signaling and vascular integrity. Dev. Cell *15*, 272–284.

Fortini, M.E., and Artavanis-Tsakonas, S. (1994). The suppressor of hairless protein participates in notch receptor signaling. Cell *79*, 273–282.

Friedländer, M.R., Chen, W., Adamidi, C., Maaskola, J., Einspanier, R., Knespel, S., and Rajewsky, N. (2008). Discovering microRNAs from deep sequencing data using miRDeep. Nat. Biotechnol. *26*, 407–415.

Galardi, S., Mercatelli, N., Giorda, E., Massalini, S., Frajese, G.V., Ciafrè, S.A., and Farace, M.G. (2007). miR-221 and miR-222 expression affects the prolif-eration potential of human prostate carcinoma cell lines by targeting p27Kip1. J. Biol. Chem. *282*, 23716–23724.

García, Z., Silio, V., Marqués, M., Cortés, I., Kumar, A., Hernandez, C., Checa, A.I., Serrano, A., and Carrera, A.C. (2006). A PI3K activity-independent func-tion of p85 regulatory subunit in control of mammalian cytokinesis. EMBO J. *25*, 4740–4751.

Geering, B., Cutillas, P.R., Nock, G., Gharbi, S.I., and Vanhaesebroeck, B. (2007). Class IA phosphoinositide 3-kinases are obligate p85-p110 hetero-dimers. Proc. Natl. Acad. Sci. USA *104*, 7809–7814.

Gerhardt, H., Golding, M., Fruttiger, M., Ruhrberg, C., Lundkvist, A., Abramsson, A., Jeltsch, M., Mitchell, C., Alitalo, K., Shima, D., and Betsholtz, C. (2003). VEGF guides angiogenic sprouting utilizing endothelial tip cell filopodia. J. Cell Biol. *161*, 1163–1177.

Ghildiyal, M., and Zamore, P.D. (2009). Small silencing RNAs: an expanding universe. Nat. Rev. Genet. *10*, 94–108.

Giraldez, A.J., Mishima, Y., Rihel, J., Grocock, R.J., Van Dongen, S., Inoue, K., Enright, A.J., and Schier, A.F. (2006). Zebrafish MiR-430 promotes deadenylation and clearance of maternal mRNAs. Science *312*, 75–79.

Graupera, M., Guillermet-Guibert, J., Foukas, L.C., Phng, L.K., Cain, R.J., Salpekar, A., Pearce, W., Meek, S., Millan, J., Cutillas, P.R., et al. (2008). Angiogenesis selectively requires the p110alpha isoform of PI3K to control endothelial cell migration. Nature *453*, 662–666.

Gregory, R.I., Chendrimada, T.P., Cooch, N., and Shiekhattar, R. (2005). Human RISC couples microRNA biogenesis and posttranscriptional gene silencing. Cell *123*, 631–640.

Gu, W., Shirayama, M., Conte, D., Jr., Vasale, J., Batista, P.J., Claycomb, J.M., Moresco, J.J., Youngman, E.M., Keys, J., Stoltz, M.J., et al. (2009). Distinct argonaute-mediated 22G-RNA pathways direct genome surveillance in the C. elegans germline. Mol. Cell *36*, 231–244.

Guo, H., Ingolia, N.T., Weissman, J.S., and Bartel, D.P. (2010). Mammalian microRNAs predominantly act to decrease target mRNA levels. Nature *466*, 835–840.

Habeck, H., Odenthal, J., Walderich, B., Maischein, H., and Schulte-Merker, S. (2002). Analysis of a zebrafish VEGF receptor mutant reveals specific disruption of angiogenesis. Curr. Biol. *12*, 1405–1412.

Hellström, M., Phng, L.K., Hofmann, J.J., Wallgard, E., Coultas, L., Lindblom, P., Alva, J., Nilsson, A.K., Karlsson, L., Gaiano, N., et al. (2007). Dll4 signalling through Notch1 regulates formation of tip cells during angiogenesis. Nature *445*, 776–780.

Hogan, B.M., Herpers, R., Witte, M., Heloterä, H., Alitalo, K., Duckers, H.J., and Schulte-Merker, S. (2009). Vegfc/Flt4 signalling is suppressed by Dll4 in developing zebrafish intersegmental arteries. Development *136*, 4001–4009.

Hutvágner, G., McLachlan, J., Pasquinelli, A.E., Bálint, E., Tuschl, T., and Zamore, P.D. (2001). A cellular function for the RNA-interference enzyme Dicer in the maturation of the let-7 small temporal RNA. Science *293*, 834–838.

Isogai, S., Lawson, N.D., Torrealday, S., Horiguchi, M., and Weinstein, B.M. (2003). Angiogenic network formation in the developing vertebrate trunk. Development *130*, 5281–5290.

Jakobsson, L., Franco, C.A., Bentley, K., Collins, R.T., Ponsioen, B., Aspalter, I.M., Rosewell, I., Busse, M., Thurston, G., Medvinsky, A., et al. (2010). Endothelial cells dynamically compete for the tip cell position during angiogenic sprouting. Nat. Cell Biol. *12*, 943–953.

Kloosterman, W.P., Wienholds, E., de Bruijn, E., Kauppinen, S., and Plasterk, R.H. (2006). In situ detection of miRNAs in animal embryos using LNA-modified oligonucleotide probes. Nat. Methods *3*, 27–29.

Kuehbacher, A., Urbich, C., Zeiher, A.M., and Dimmeler, S. (2007). Role of Dicer and Drosha for endothelial microRNA expression and angiogenesis. Circ. Res. *101*, 59–68.

Lee, Y., Ahn, C., Han, J., Choi, H., Kim, J., Yim, J., Lee, J., Provost, P., Rådmark, O., Kim, S., and Kim, V.N. (2003). The nuclear RNase III Drosha initiates microRNA processing. Nature *425*, 415–419.

Leslie, J.D., Ariza-McNaughton, L., Bermange, A.L., McAdow, R., Johnson, S.L., and Lewis, J. (2007). Endothelial signalling by the Notch ligand Delta-like 4 restricts angiogenesis. Development *134*, 839–844.

Lobov, I.B., Renard, R.A., Papadopoulos, N., Gale, N.W., Thurston, G., Yancopoulos, G.D., and Wiegand, S.J. (2007). Delta-like ligand 4 (Dll4) is induced by VEGF as a negative regulator of angiogenic sprouting. Proc. Natl. Acad. Sci. USA *104*, 3219–3224.

Lyons, D.A., Pogoda, H.M., Voas, M.G., Woods, I.G., Diamond, B., Nix, R., Arana, N., Jacobs, J., and Talbot, W.S. (2005). erbb3 and erbb2 are essential for schwann cell migration and myelination in zebrafish. Curr. Biol. *15*, 513–524.

Nicoli, S., Standley, C., Walker, P., Hurlstone, A., Fogarty, K.E., and Lawson, N.D. (2010). MicroRNA-mediated integration of haemodynamics and Vegf signalling during angiogenesis. Nature *464*, 1196–1200.

Park, S.Y., Lee, J.H., Ha, M., Nam, J.W., and Kim, V.N. (2009). miR-29 miRNAs activate p53 by targeting p85 alpha and CDC42. Nat. Struct. Mol. Biol. *16*, 23–29.

Poliseno, L., Tuccoli, A., Mariani, L., Evangelista, M., Citti, L., Woods, K., Mercatanti, A., Hammond, S., and Rainaldi, G. (2006). MicroRNAs modulate the angiogenic properties of HUVECs. Blood *108*, 3068–3071.

Poole, T.J., and Coffin, J.D. (1989). Vasculogenesis and angiogenesis: two distinct morphogenetic mechanisms establish embryonic vascular pattern. J. Exp. Zool. *251*, 224–231.

Rand, T.A., Ginalski, K., Grishin, N.V., and Wang, X. (2004). Biochemical identification of Argonaute 2 as the sole protein required for RNA-induced silencing complex activity. Proc. Natl. Acad. Sci. USA *101*, 14385–14389.

Siekmann, A.F., and Lawson, N.D. (2007). Notch signalling limits angiogenic cell behaviour in developing zebrafish arteries. Nature *445*, 781–784.

Suárez, Y., and Sessa, W.C. (2009). MicroRNAs as novel regulators of angiogenesis. Circ. Res. *104*, 442–454.

Suárez, Y., Fernández-Hernando, C., Yu, J., Gerber, S.A., Harrison, K.D., Pober, J.S., Iruela-Arispe, M.L., Merkenschlager, M., and Sessa, W.C. (2008). Dicer-dependent endothelial microRNAs are necessary for postnatal angiogenesis. Proc. Natl. Acad. Sci. USA *105*, 14082–14087.

Suchting, S., Freitas, C., le Noble, F., Benedito, R., Bréant, C., Duarte, A., and Eichmann, A. (2007). The Notch ligand Delta-like 4 negatively regulates endothelial tip cell formation and vessel branching. Proc. Natl. Acad. Sci. USA *104*, 3225–3230.

Tammela, T., Zarkada, G., Wallgard, E., Murtomäki, A., Suchting, S., Wirzenius, M., Waltari, M., Hellström, M., Schomber, T., Peltonen, R., et al. (2008). Blocking VEGFR-3 suppresses angiogenic sprouting and vascular network formation. Nature *454*, 656–660.

Thurston, G., Noguera-Troise, I., and Yancopoulos, G.D. (2007). The Delta paradox: DLL4 blockade leads to more tumour vessels but less tumour growth. Nat. Rev. Cancer *7*, 327–331.

Vanhaesebroeck, B., Guillermet-Guibert, J., Graupera, M., and Bilanges, B. (2010). The emerging mechanisms of isoform-specific PI3K signalling. Nat. Rev. Mol. Cell Biol. *11*, 329–341.

Wang, J.F., Zhang, X., and Groopman, J.E. (2004). Activation of vascular endothelial growth factor receptor-3 and its downstream signaling promote cell survival under oxidative stress. J. Biol. Chem. *279*, 27088–27097.

Wang, S., Aurora, A.B., Johnson, B.A., Qi, X., McAnally, J., Hill, J.A., Richardson, J.A., Bassel-Duby, R., and Olson, E.N. (2008). The endothelial-specific microRNA miR-126 governs vascular integrity and angiogenesis. Dev. Cell *15*, 261–271.

Wu, L., Fan, J., and Belasco, J.G. (2006). MicroRNAs direct rapid deadenylation of mRNA. Proc. Natl. Acad. Sci. USA *103*, 4034–4039.

Wu, Y.H., Hu, T.F., Chen, Y.C., Tsai, Y.N., Tsai, Y.H., Cheng, C.C., and Wang, H.W. (2011). The manipulation of microRNA-gene regulatory networks by KSHV induces endothelial cell motility. Blood *118*, 2896–2905.

Yu, J., Zhang, Y., McIlroy, J., Rordorf-Nikolic, T., Orr, G.A., and Backer, J.M. (1998). Regulation of the p85/p110 phosphatidylinositol 3′-kinase: stabilization and inhibition of the p110alpha catalytic subunit by the p85 regulatory subunit. Mol. Cell. Biol. *18*, 1379–1387.

Zhu, N., Zhang, D., Chen, S., Liu, X., Lin, L., Huang, X., Guo, Z., Liu, J., Wang, Y., Yuan, W., and Qin, Y. (2011). Endothelial enriched microRNAs regulate angiotensin II-induced endothelial inflammation and migration. Atherosclerosis *215*, 286–293.

Zygmunt, T., Gay, C.M., Blondelle, J., Singh, M.K., Flaherty, K.M., Means, P.C., Herwig, L., Krudewig, A., Belting, H.G., Affolter, M., et al. (2011). Semaphorin-PlexinD1 signaling limits angiogenic potential via the VEGF decoy receptor sFlt1. Dev. Cell *21*, 301–314.